

## Article

# Modeling of Dry Reforming of Methane Using Artificial Neural Networks

Mohammod Hafizur Rahman <sup>1</sup>  and Mohammad Biswas <sup>2,\*</sup> <sup>1</sup> Chemical Engineering Department, College of Engineering, Imam Mohammad Ibn Saud Islamic University, Riyadh 11432, Saudi Arabia; mhalrahman@imamu.edu.sa<sup>2</sup> Department of Mechanical Engineering, College of Engineering, The University of Texas at Tyler, Houston, TX 77082, USA

\* Correspondence: mbiswas@uttyler.edu

**Abstract:** The process of dry reforming methane (DRM) is seen as a viable approach for producing hydrogen and lowering the atmospheric concentration of carbon dioxide. Recent times have witnessed notable advancements in the development of catalysts that enable this pathway. Numerous experiments have been conducted to investigate the use of nickel-based catalysts in the dry reforming of methane. All these reported experiments showed that variations in the catalyst property, namely pore size, pore volume, and surface area, affect the hydrogen production in DRM. None of the previous studies has modeled the surface nickel-incorporated catalyst activity based on its properties. In this research, DRM's hydrogen yield is predicted using three different artificial neural network-learning algorithms as a function of the physical properties of Ni-based catalyst along with two reaction inputs. The geometric properties as an input set are a different approach to developing such empirical models. The best-fitting models are the artificial neural network model using the Levenberg–Marquardt algorithm and ten hidden neurons, which gave a coefficient of determination of 0.9931 and an MSE of 7.51, and the artificial neural network model using the scaled conjugate gradient algorithm and eight hidden layer neurons, which had a coefficient of determination of 0.9951 and an MSE of 4.29. This study offers useful knowledge on how to improve the DRM processes.

**Keywords:** dry reforming of methane; machine learning; hydrogen yield; physical properties of nickel-based catalyst; artificial neural network



**Citation:** Rahman, M.H.; Biswas, M. Modeling of Dry Reforming of Methane Using Artificial Neural Networks. *Hydrogen* **2024**, *5*, 800–818. <https://doi.org/10.3390/hydrogen5040042>

Received: 12 September 2024

Revised: 29 October 2024

Accepted: 5 November 2024

Published: 7 November 2024



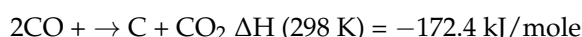
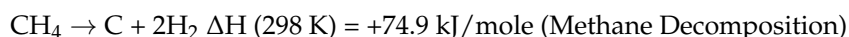
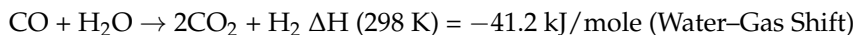
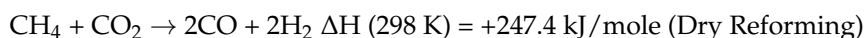
**Copyright:** © 2024 by the authors. Licensee MDPI, Basel, Switzerland. This article is an open access article distributed under the terms and conditions of the Creative Commons Attribution (CC BY) license (<https://creativecommons.org/licenses/by/4.0/>).

## 1. Introduction

Research on hydrogen generation is ongoing because it has the potential to improve energy security, address important environmental and energy-related issues, and generate new business opportunities. Hydrogen is a promising energy alternative for the future because of its clean energy benefits [1]. The most desirable approach to producing hydrogen among the various technologies available is through dry methane reforming of methane. The urgency of finding a solution to lower carbon dioxide and methane emissions from the atmosphere increased along with the severity of the global warming crisis [2].

The most economical way of producing hydrogen is steam reforming of methane (SRM). It is the most widely used method for hydrogen production; about half of total hydrogen is generated through this method. The drawback of this process is that it produces greenhouse gases (GHGs). This is why the modern trend is to find an alternative way of producing hydrogen. Many researchers have turned their attention to producing hydrogen using the dry reformation of methane (DRM), as it effectively valorizes both methane and carbon dioxide. The process of turning methane (CH<sub>4</sub>) and carbon dioxide (CO<sub>2</sub>) into syngas—a combination of hydrogen (H<sub>2</sub>) and carbon monoxide (CO)—is called DRM, also referred to as CO<sub>2</sub> reforming of methane [3,4].

The process of DRM is seen as a viable approach for producing hydrogen and lowering the atmospheric concentration of carbon dioxide. Nonetheless, its main challenge is its high energy requirements. DRM's main reactions are given below.



Being an endothermic reaction, DRM needs elevated temperatures to function properly—usually between 700 °C and 1000 °C. When compared to other syngas manufacturing procedures, this process is less cost-effective and energy-efficient due to the requirement for high temperatures, which also results in high energy usage [5–9].

Noteworthy progress has been made in the creation of catalysts that facilitate this pathway in recent times. For DRM, noble metal catalysts are particularly useful. Examples of these include those containing ruthenium (Ru), platinum (Pt), rhodium (Rh), and palladium (Pd). These catalysts exhibit high levels of stability, coking resistance, and activity [10]. Non-noble metals, especially nickel (Ni), are widely used in DRM because of their low cost. The employment of catalysts based on nickel in the dry reforming of methane has been the subject of numerous experiments. Ni-based catalysts can achieve sufficient activity for DRM if they are supported by the right materials (such as MgO, Al<sub>2</sub>O<sub>3</sub>, or CeO<sub>2</sub>) [10–14]. The supporting metal oxides yield enhanced performance and increased catalytic stability. It promotes the anchoring of the active phase to their surface. This generally leads to increased conversions and selectivity in the DRM reaction [15,16]. A catalytic support, while not directly involved in the process, can modify the overall properties of the catalyst. Numerous prior studies have demonstrated that the catalytic performance of metallic catalysts is enhanced with the dispersion of the active support and the metal. Moreover, the support must provide exceptional thermal stability and superior mechanical strength [17,18].

Pore volume, surface area, and pore diameter always affect the catalytic activity. These properties influence the interaction of the reactants with the active sites of the catalyst, influencing the total effectiveness of the catalytic process [17]. The appropriate calcination technique and optimal matrix combination with Ni during the manufacturing of catalysts can influence the morphology of the solid heterogeneous Ni-based catalyst [19–22]. The pore diameter and surface area of a Ni catalyst in DRM significantly influence hydrogen yield. Catalysts with higher pore volume tend to exhibit improved performance in DRM, attributed to enhanced mass transfer and reduced coking. Catalysts with mesoporous structures typically exhibit enhanced activity and improved hydrogen selectivity [23]. The diameter of the pores influences the quantity of carbon dioxide and methane that can access the active sites of the catalyst. When the holes are excessively small, reactant molecules are unable to penetrate, thereby restricting the reaction to the surface area. When pore sizes are suitable, the movement of reactants and products is enhanced. Smaller pores can lead to diffusion restrictions despite the fact that larger openings may decrease the distance molecules need to traverse to access active sites. The influence of pore diameter on carbon deposition and generation is a prevalent concern in DRM. Optimal pore widths can reduce carbon buildup by allowing sufficient space for carbon species to be gasified and eliminated [24,25].

The ability of a catalyst to efficiently catalyze the reaction between methane (CH<sub>4</sub>) and carbon dioxide (CO<sub>2</sub>) to produce syngas (H<sub>2</sub> and CO) is measured by its hydrogen yield, which is a critical performance metric for assessing the catalytic activity of different catalysts.

By comparing the hydrogen yields of different catalysts under similar conditions, the performance of a catalyst can be determined [26]. Hydrogen yield is calculated as follows:

$$\text{Hydrogen yield(\%)} = \frac{\text{Moles of H}_2 \text{ in production}}{2 \times \text{Moles of CH}_4 \text{ in feed}} \times 100$$

An artificial neural network (ANN) can model any complex non-linear phenomenon [27,28]. It is made up of networked neurons that allow the processing of a set of input data to produce matching sets of desired outputs [29]. Previously, ANN was chosen by testing different neural network topologies based on the non-linear relationship between the reaction temperature, catalyst weight, time of stream, calcination temperature, calcination time, specific volume, and H<sub>2</sub> yield [30,31]. Hossain et al. [31] developed an ANN model to predict hydrogen yield, CO yield, methane, and carbon dioxide conversions as a function of feed ratio, temperature, and metal loading. Similarly, Alsaffar et al. [30] developed an ANN model to predict H<sub>2</sub> and CO production as a function of inlet pressures and temperature. Gendy et al. [32] developed several models, including ANN models for the DRM process, and they obtained an excellent fit for ANN models to predict the performance for operating conditions of gas velocity, temperature, and composition. In contrast to prior research on ANN modeling for dry methane reforming, this article presents a model utilizing published experimental data, incorporating various geometric properties of Ni-based catalysts as input variables, alongside temperature and gas velocity, to generate hydrogen from methane without the presence of water.

This study looked to develop a model using surface area, pore specific volume, and pore diameter as input variables, which has not been carried out in the previous literature and would be of interest to carry out in potentially optimized reactors and determine relevant performance. To understand the variables, a broader understanding of the influence of these variables affecting H<sub>2</sub> generation can be observed to improve the overall impact on the reaction process. The work in this paper is outlined as follows: Section 1 introduces the topic of dry reforming of methane along with blackbox modeling based on ANN, the next section explains the modeling approach and relevant learning algorithms, the following section presents resulting ANN models and discussion compared to the experimental data, and Section 4 provides the concluding points and potential implication.

## 2. Materials and Methods

### 2.1. Artificial Neural Network Modeling

ANN is like the human central nervous network. Such blackbox modeling techniques have extended and increased over the past decade or more due to significant progress in evaluating complicated and big challenges through the use of innovative tools and computational ability [33,34]. Figure 1 shows an ANN static fitting layout to involve the input variable, neurons, along with weight and bias, and the output [35]. The neuron is connected through a weight function, added to a bias parameter, to go through an activation function. Figure 1 illustrates the layout for the ANN modeling technique, with input vector **I** and output layer vector **O**. The input vector goes into a matrix of weight **W<sup>I</sup>** and is added to a matrix of bias **b<sup>I</sup>** to then go through the hidden layer activation function  $f(\cdot)$ , which is a log-sigmoid function. The output layer obtains values through hidden neurons. The value from the hidden layer goes to a matrix of output weight **W<sup>O</sup>** and is then added to a matrix of output bias **b<sup>O</sup>** to then be followed by the output activation function  $f(\cdot)$ , which is a linear function. Furthermore, the number of hidden neurons can be varied to obtain the optimal model. The values of the addition, along with the values of activation functions, provide results in the last two layers for the given ANN layout.

For model validation and training, the literature data were collected from various sources. Extracted data are shown in Tables 1 and 2. Table 3 presents the summary of major variables for the model development and analysis.

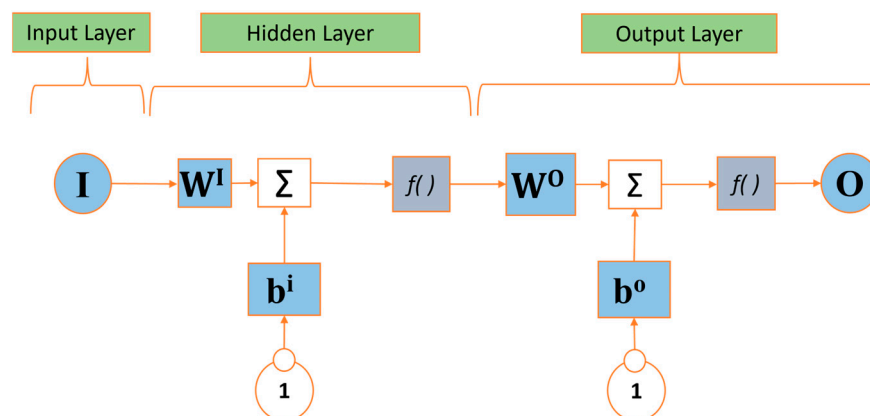


**Figure 1.** Layout of the ANN structure.

**Table 1.** Experimental data extracted from the dry reforming of methane tests.

Sr/No	Catalyst Name	Ni wt. %	CW(g)	Y (H <sub>2</sub> ) %	Reference
1	Ni/ZrO <sub>2</sub>	7.65	0.15	29	[36]
2	5Ni15YZr	5	0.1	55	[37]
3	5Ni-SP-OA	5	0.1	45	[7]
4	Ni-SP-Imp	5	0.1	32	[7]
5	Ni-20/MSN	5	0.1	71	[5]
6	10NiRh/Al <sub>2</sub> O <sub>3</sub>	10	0.05	35	[38]
7	10NiRh/Al <sub>2</sub> O <sub>3</sub>	10	0.05	45	[38]
8	NiY/Al <sub>2</sub> O <sub>3</sub>	10	0.05	11	[38]
9	Ni/CeO <sub>2</sub>	5	0.15	57	[39]
10	Ni/CeO <sub>2</sub> -Al <sub>2</sub> O <sub>3</sub>	10	—	12	[2]
11	NiPd-SiO <sub>2</sub> -Imp	7.5	0.1	36	[7]
12	NiPd-SiO <sub>2</sub> -OA	7.5	0.1	63	[7]
13	5Ni2Ce/ZSM5	5	0.15	35	[40]
14	5Ni2Ce/ZSM5	5	0.15	27	[40]
15	5Ni2Ce/ZSM5	5	0.15	68	[40]
16	NZA-0C	5	0.1	74	[14]
17	NZA-1C	5	0.1	78	[14]
18	NZA-2C	5	0.1	80	[14]
19	NZA-3C	5	0.1	84	[14]
20	NZA-4C	5	0.1	82	[14]
21	Ni/TiO <sub>2</sub> -600	5	0.1	26	[22]
22	Ni/TiO <sub>2</sub> -800	5	0.1	22	[22]
23	Ni/MgO-600	5	0.1	55	[22]
24	Ni/MgO-800	5	0.1	35	[22]
25	Ni/Al <sub>2</sub> O <sub>3</sub> -600	5	0.1	58	[22]
26	Ni/Al <sub>2</sub> O <sub>3</sub> -800	5	0.1	58	[22]
27	Ni/ZrO <sub>2</sub> -600	5	0.1	45	[22]
28	Ni/ZrO <sub>2</sub> -800	5	0.1	46	[22]

**Table 2.** Properties selected as input variables for ANN modeling.

Sr/No	Catalyst Name	Surface Area (m <sup>2</sup> /g)	Pore Volume (cm <sup>3</sup> /g)	Pore Diameter (nm)	GHSV (L/h gcat)	RT (°C)
1	Ni/ZrO <sub>2</sub>	44	0.05	19.9	40	800
2	5Ni15YZr	25	0.18	24	42	700
3	5Ni-SP-OA	290.3	0.6614	9.11	24	700
4	Ni-SP-Imp	296.1	0.7414	10.67	24	700
5	Ni-20/MSN	422	0.645	10.22	36	700
6	10NiRh/Al <sub>2</sub> O <sub>3</sub>	183	0.53	11.9	100	550
7	10NiRh/Al <sub>2</sub> O <sub>3</sub>	183	0.53	11.9	100	650
8	NiY/Al <sub>2</sub> O <sub>3</sub>	163	0.66	17.17	60	550
9	Ni/CeO <sub>2</sub>	83.1	0.14	4.85	40	700
10	Ni/CeO <sub>2</sub> -Al <sub>2</sub> O <sub>3</sub>	100.6	0.324	40.75	30	750
11	NiPd-SiO <sub>2</sub> -Imp	271.3	0.7236	10.67	24	700
12	NiPd-SiO <sub>2</sub> -OA	278.1	0.635	8.83	24	700
13	5Ni2Ce/ZSM5	235	0.09	5.4	42	700
14	5Ni2Ce/ZSM5	235	0.09	5.4	42	700
15	5Ni2Ce/ZSM5	235	0.09	5.4	42	800
16	NZA-0C	124.4	0.59	19	42	800
17	NZA-1C	119.5	0.57	18.8	42	800
18	NZA-2C	117.5	0.56	18.9	42	800
19	NZA-3C	117.8	0.55	18.7	42	800
20	NZA-4C	115.2	0.54	18.8	42	800
21	Ni/TiO <sub>2</sub> -600	34.77	0.33	36.7	42	700
22	Ni/TiO <sub>2</sub> -800	3.04	0.032	51.2	42	700
23	Ni/MgO-600	55.2	0.52	35.4	42	700
24	Ni/MgO-800	37.12	0.35	40	42	700
25	Ni/Al <sub>2</sub> O <sub>3</sub> -600	196	0.61	9.71	42	700
26	Ni/Al <sub>2</sub> O <sub>3</sub> -800	175.29	0.67	11.2	42	700
27	Ni/ZrO <sub>2</sub> -600	23.75	0.21	29.17	42	700
28	Ni/ZrO <sub>2</sub> -800	14.13	0.14	44.41	42	700

**Table 3.** Dry reforming of methane reactor variables considered in this study.

Variable	Range	Units
GSHV (Input)	24 to 100	L/h gcat
Reactor Temperature (Input)	550 to 800	°C
Surface Area (Input)	0.44 to 422	m <sup>2</sup> /g
Pore Volume (Input)	0.03 to 0.74	cm <sup>3</sup> /g
Pore Diameter (Input)	4 to 52	Nm
Hydrogen Yield (Output)	1 to 100	%

For the training part of the model development, values for the output layer are determined from the input layer values. The goal is to minimize the error between the trained model's predictions and the actual output data. When there is a significant discrepancy in the model's predictions, an iterative method is used. The model's parameters are updated until the error is reduced to the desired level. This process aims to continuously improve the model's accuracy in handling complex systems. After training, ANN retains the optimized weights and biases for future validation. These parameters are vital as they encapsulate the knowledge gained from the training data. During validation, the ANN utilizes these approximate weights and biases to evaluate its performance on new, unseen data based on the given parameters. Utilizing the learned parameters, the ANN model can accurately predict data beyond the training phase. During decision-making, the model detects patterns with untrained parameters that align with the overall training goals. The model independently analyzes data to uncover meaningful relationships without any prior knowledge. This allows it to derive insights into decision-making patterns based solely on the training data. There are several methods available to significantly reduce

the error margin between predicted and experimental data. However, the selection of the appropriate approach depends on the user's judgment and specific requirements. One example of such an approach is the mean squared error (MSE) depicted in Equation (1), a commonly used metric for evaluating prediction model performance with a 95% confidence interval. The right method to choose depends on the user's comprehension of the problem and the specific needs for enhancing prediction accuracy.

$$MSE = \frac{1}{p} \sum (T - Z)^2 \quad (1)$$

Data points occurring are denoted as  $p$ , prediction as  $T$ , and empirical data as  $Z$  [19]. Errors are useful in calculating the coefficient of determination. Equation (2) reviews the coefficient of determination  $R^2$  mathematically.

$$R^2 = [Cor(T, Z)]^2 = 1 - \frac{\sum (T - Z)^2}{\sum (Z - \bar{Z})^2} \quad (2)$$

The correlation coefficient is  $Cor(T, Z)$ .  $\bar{Z}$  is the data averaged, and the sum of squares is  $\sum (Z - \bar{Z})^2$ .

The range of  $R^2$  is from zero to one with a 95% confidence interval. A coefficient of determination of 0.85 implies that 85% of the variability is explained by predictor factors, ideal for exceptional fit. To achieve a well-fitted model, it undergoes rapid training and error margin reduction. Quick convergence requires training the ANN using Newton's method, even when the Hessian matrix is singular [41]. The Levenberg–Marquardt (LM) algorithm offers an alternative approach to the Hessian matrix, effectively addressing related concerns. In LM, another term,  $\mu I$ , is included to enhance conditioning. Detailed investigations have been conducted to establish suitable values for  $\mu$  [42]. When values of  $\mu$  are lesser, Newton's algorithm is reached; when values of  $\mu$  are bigger, there is a decrease in the gradient.

Conversely, the scaled conjugate gradient (SCG) algorithm utilizes conjugate directions and does not perform a search at every iteration [43]. To run similar simulations, there is a higher cost compared to other approaches. SCG was formed to eliminate the need for challenging line searches. When SCG is employed, the MATLAB® (version 9.0) function 'trainscg' adjusts the ANN bias and weight values [44]. The size of each step is estimated with the aid of separate techniques. Equation (3) shows the term in second order:

$$\bar{S}_n = \frac{E'(\bar{\omega}_n + \sigma_n \bar{p}_n) - E'(\bar{\omega}_n)}{\sigma k} + \lambda_n \bar{p}_n \quad (3)$$

where  $\lambda_n$  is the scalar unit and is subjected to the sign of  $\sigma n$ .

$$\alpha_n = \frac{\mu_n}{\delta_n} = \frac{-\bar{p}_j^T E'_{q\omega}(\bar{z}_1)}{\bar{p}_j^T E''(\bar{\omega}) \bar{p}_j} \quad (4)$$

$\bar{\omega}$  represents the vector in space  $R^n$ ,  $E\bar{\omega}$  denotes the global error function,  $E'\bar{\omega}$  is the gradient of error,  $E'_{q\omega}(\bar{z}_1)$  is the quadratic approximation, and  $\bar{p}_1, \bar{p}_2, \dots, \bar{p}_n$  are weight vectors.

The term  $\lambda_n$  can be revised using Equation (5):

$$\bar{\lambda}_n = 2 \left( \lambda_n - \frac{\delta_n}{|p_n^2|} \right) \quad (5)$$

when  $\Delta_n > 0.75$ , then  $\lambda_n = \frac{\lambda_n}{4}$ , and when  $\Delta_n < 0.25$ , then  $\lambda_n = \lambda_n + \frac{\delta_n(1-\Delta_n)}{|p_n^2|}$ .

The term  $\Delta_n$  is a comparative value, deduced using Equation (6):

$$\Delta_n = \frac{2\delta_n[E(\bar{\omega}_n) - E(\bar{\omega}_n + \alpha_n \bar{p}_n)]}{\mu_n^2} \quad (6)$$

The Bayesian regularization (BR) algorithm considers the Hessian matrix in another way [27]. Equation (7) represents the objective function:

$$G = \alpha E_w + \beta E_D \quad (7)$$

The BR considers weight in relation to the network as subjectively selected parameters. Equation (8) is the probability function for an array  $w$ :

$$g(wD, \alpha, \beta, M) = \frac{g(Dw, \beta, M)g(w\alpha, M)}{g(D\alpha, \beta M)} \quad (8)$$

The term  $M$  represents the ANN model used.  $g(w\alpha, M)$  is the prior density, and  $g(Dw, \beta, M)$  is the likelihood function.

## 2.2. Computational Resources for ANN Models

When artificial neural network (ANN) models are developed and trained for predicting hydrogen yield in dry reforming of methane (DRM) using MATLAB's Neural Network Toolbox<sup>®</sup>, here are a couple of key computational resources that were considered:

1. Processing Time—The time required to train an ANN model can vary significantly based on the complexity of the network (e.g., number of layers and neurons), the size of the dataset, and the computational power available. For this study, training a simple feedforward network with several hidden neurons took a few minutes on a standard CPU with Windows 11 operating system.

2. Memory Requirements—Training ANNs can be memory-intensive, so the memory required depends on the size of the dataset, the architecture of the network, and the batch size used during training. For this study, training a network with several parameters on a small dataset requires less than 2 GB of RAM on a standard CPU.

## 3. Resulting Outcome and Discussions

The fit of the ANN time series model was evaluated using the MATLAB Deep Learning Toolbox<sup>®</sup>, which is presented in Figure 2. Five input variables and one output variable of hydrogen yield have been considered for this work. The models utilized more than 90% of twenty-eight data points for training the model and less than 10% for model testing and validation. The number of hidden layer neurons and the type of learning algorithm were adjusted to create different models to aim to identify the best fit. Table 4 presents a comparison of the three different algorithms of the ANN static model using the  $R^2$  and the mean squared error. In Table 4, the type of algorithm is shown in Column 1, the count of hidden neurons is presented in Column 2, the  $R^2$  results are in Column 3, and the mean squared error values are in Column 4. Figures 3–5 show the experimental and model responses of the hydrogen yield for the ANN models with 5, 10, 30, and 50 hidden neurons and using LM as a function of surface area, pore diameter, and volume. Figures 6–8 present the experimental and model data for hydrogen yield in ANN models with varying hidden neurons, using BR as a function of surface area, pore diameter, and volume. Figures 9–11 show the experimental and model data of the hydrogen yield for the ANN models with varying hidden neurons using SCG as a function of surface area, pore diameter, and volume. In Figures 3–12, the y-axis is the hydrogen yield in %, and the x-axis is one of the three input variables: surface area, pore volume, and pore diameter.



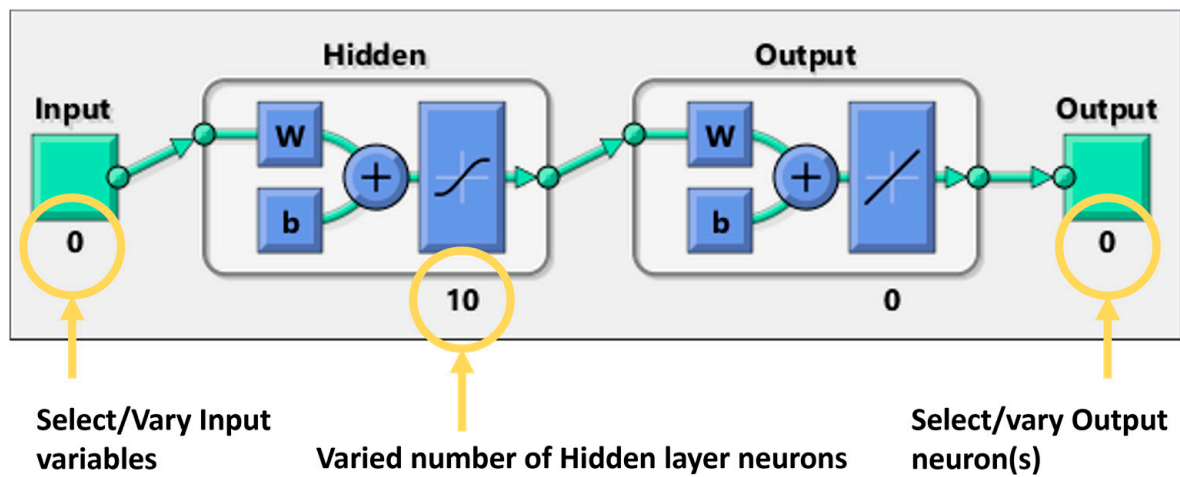
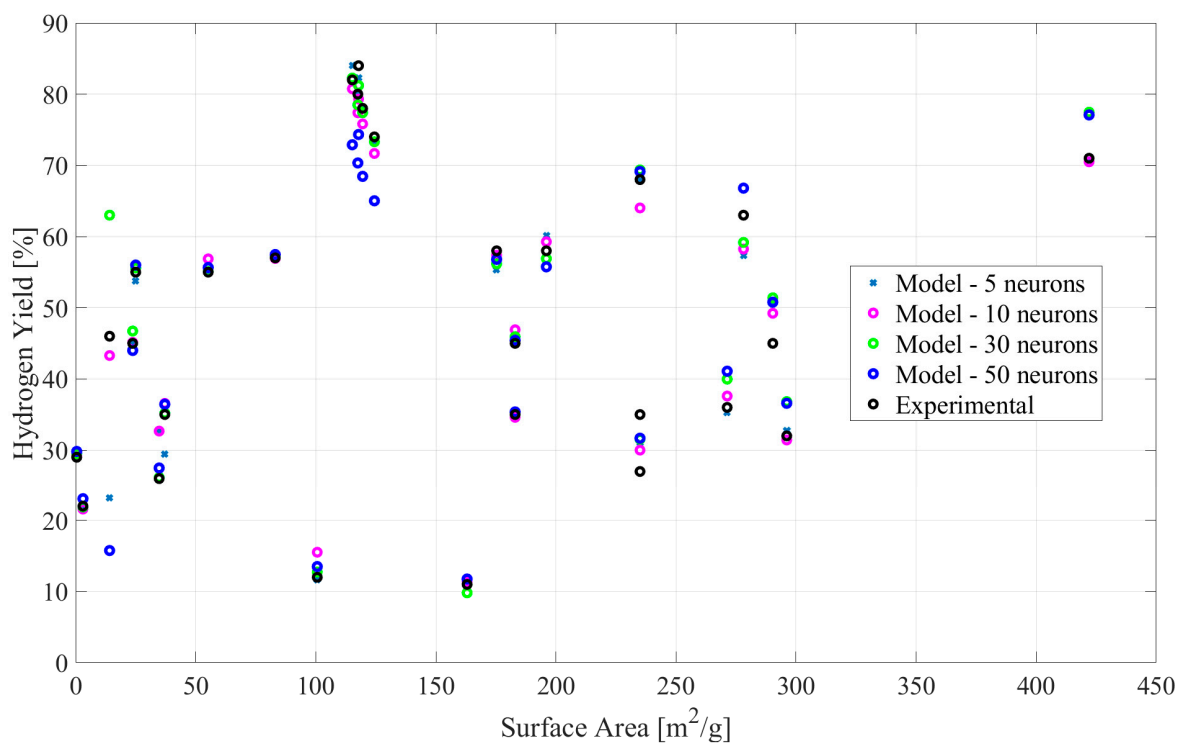


Figure 2. Layout of ANN modeling approach in MATLAB Deep Learning Toolbox®.

Table 4. Evaluation and contrast of selected ANN model results.

Type of Learning Algorithm	Number of Hidden Neurons	Coefficient of Determination	Mean Squared Error
LM	1	0.8220	142.8
LM	5	0.9719	25.49
LM	10	0.9931	7.51
LM	12	0.9785	19.37
LM	17	0.9718	26.46
LM	30	0.9816	17.2
LM	40	0.8872	93.34
LM	50	0.9375	55.01
SCG	1	0.3943	377.5
SCG	5	0.9396	59.59
SCG	8	0.9951	4.29
SCG	10	0.9587	37.16
SCG	12	0.8982	155.0
SCG	15	0.9764	21.01
SCG	17	0.9868	12.60
SCG	20	0.8465	192.4
BR	1	0.7652	180.7
BR	5	0.9604	35.33
BR	8	0.7697	177.2
BR	10	0.7665	179.4
BR	12	0.7664	179.4
BR	15	0.7666	179.2
BR	17	0.7667	179.2
BR	20	0.7668	179.1





**Figure 3.** Experimental and ANN models using LM results of hydrogen yield as a function of surface area.

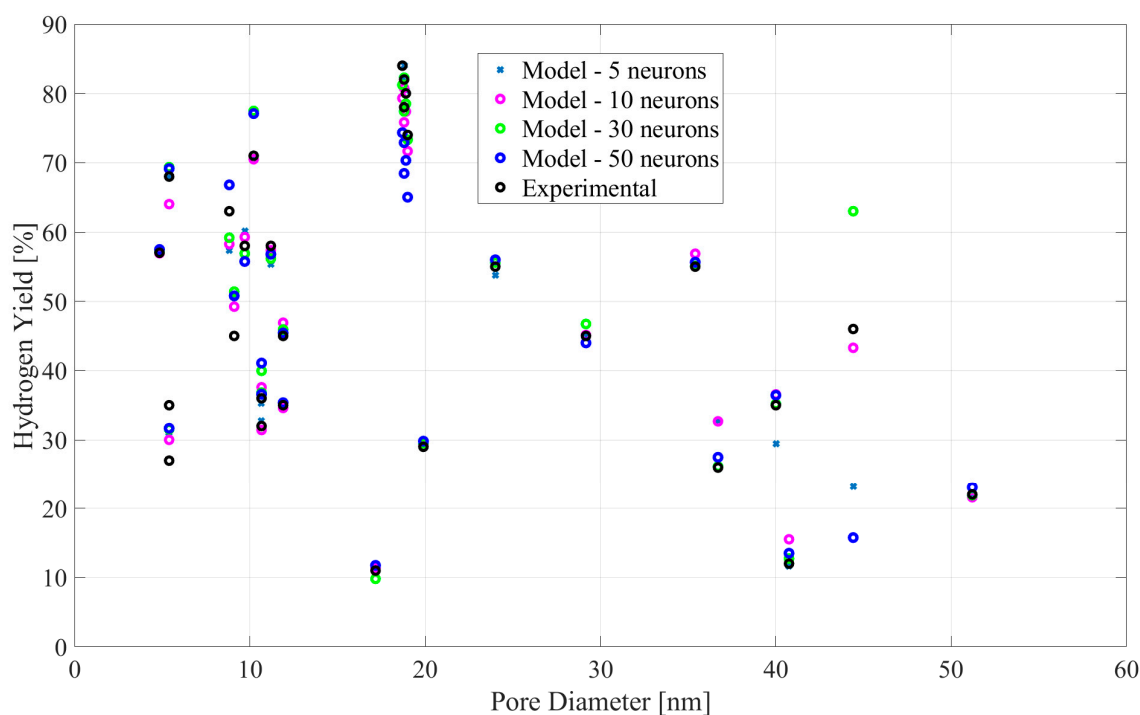


**Figure 4.** Experimental and ANN models using LM results of hydrogen yield as a function of pore diameter.

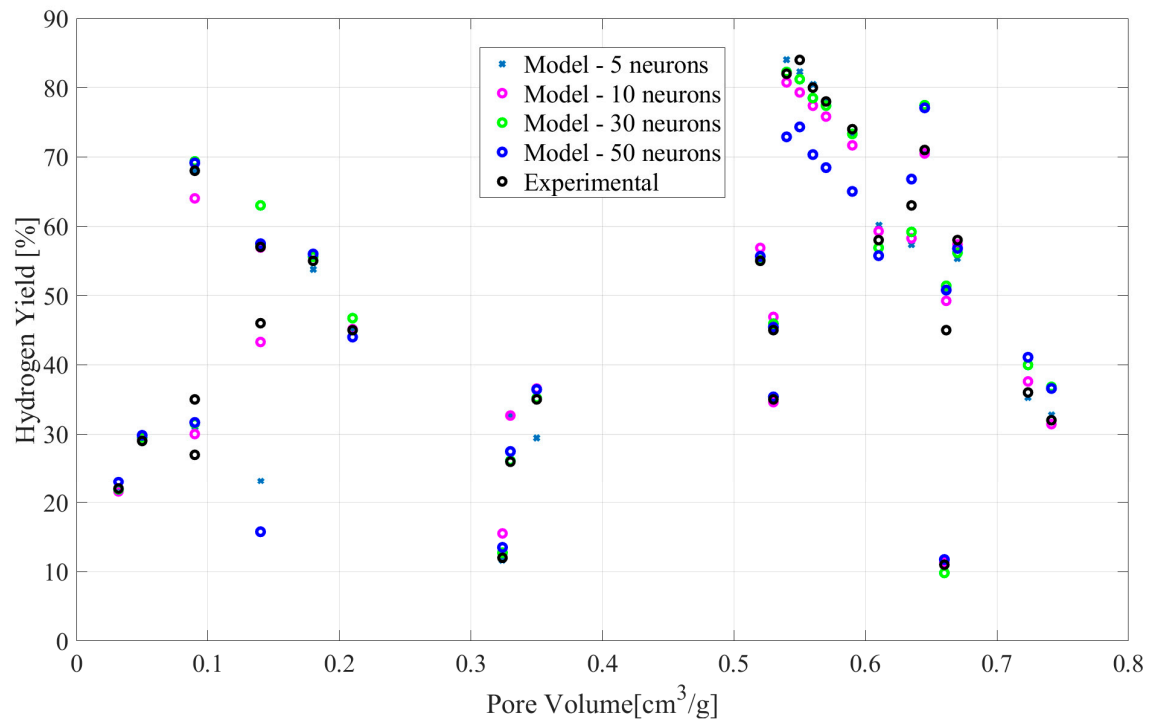


**Figure 5.** Experimental and ANN models using LM results of hydrogen yield as a function of pore volume.

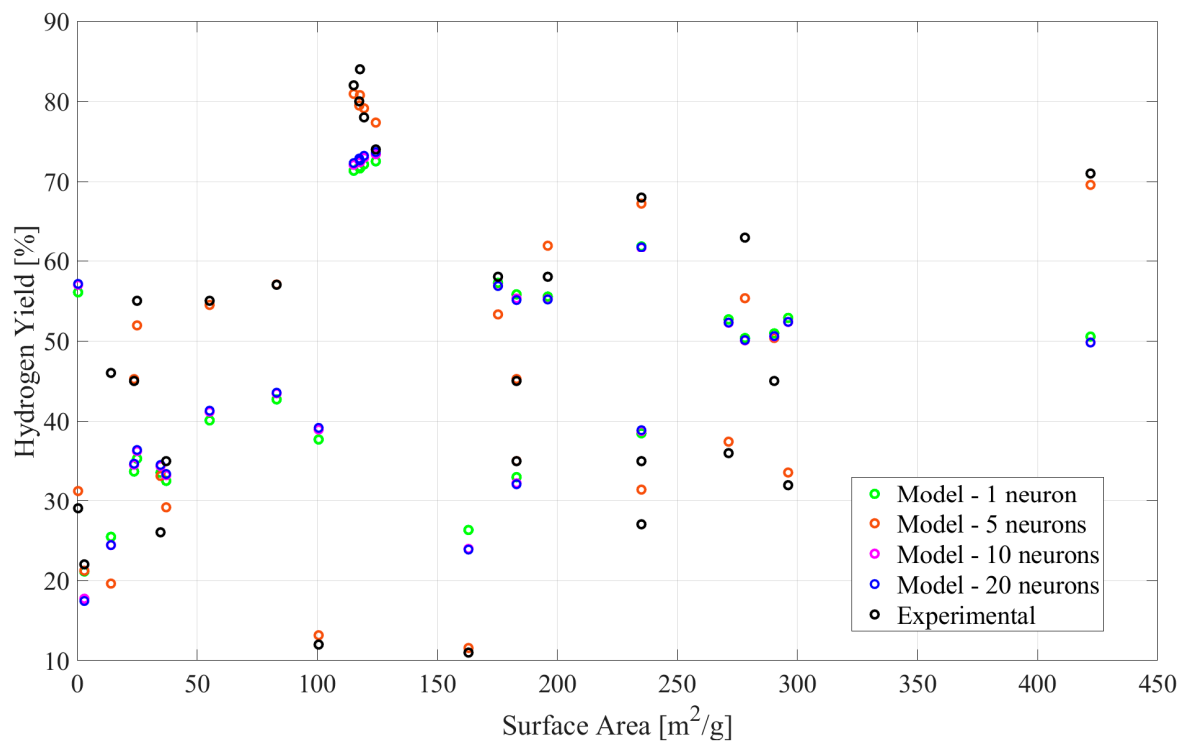


**Figure 6.** Experimental and ANN models using BR results of hydrogen yield as a function of surface area.

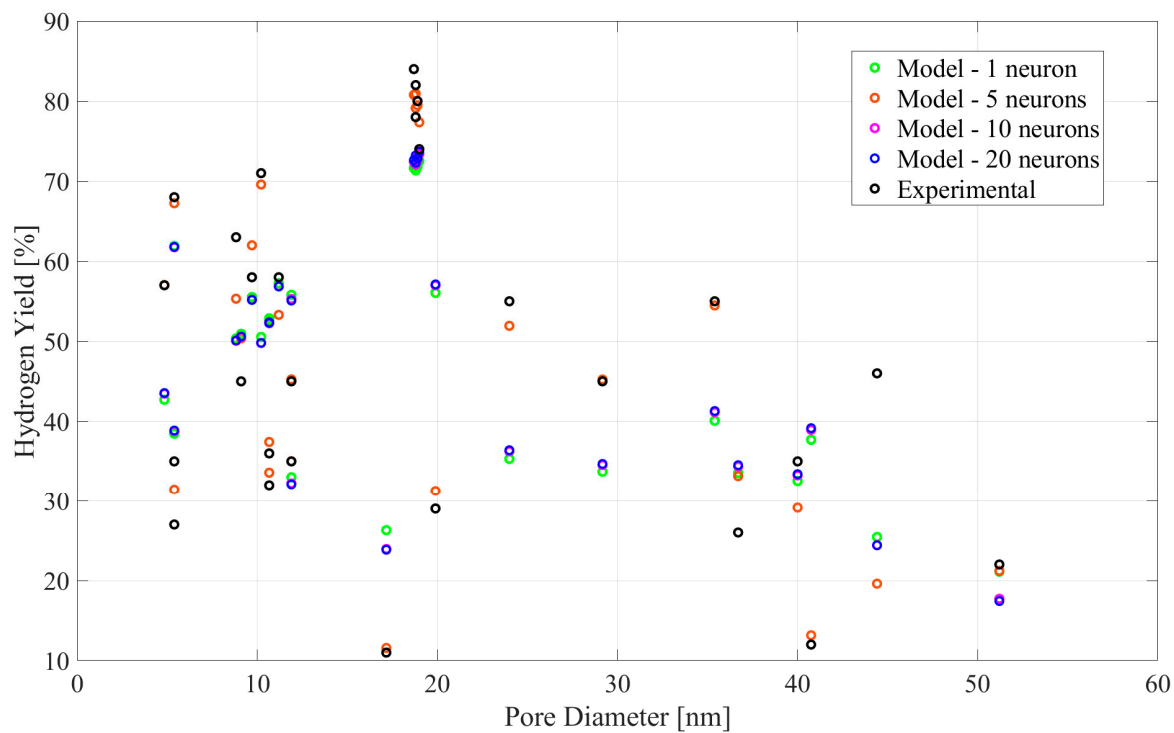


**Figure 7.** Experimental and ANN models using BR results of hydrogen yield as a function of pore diameter.

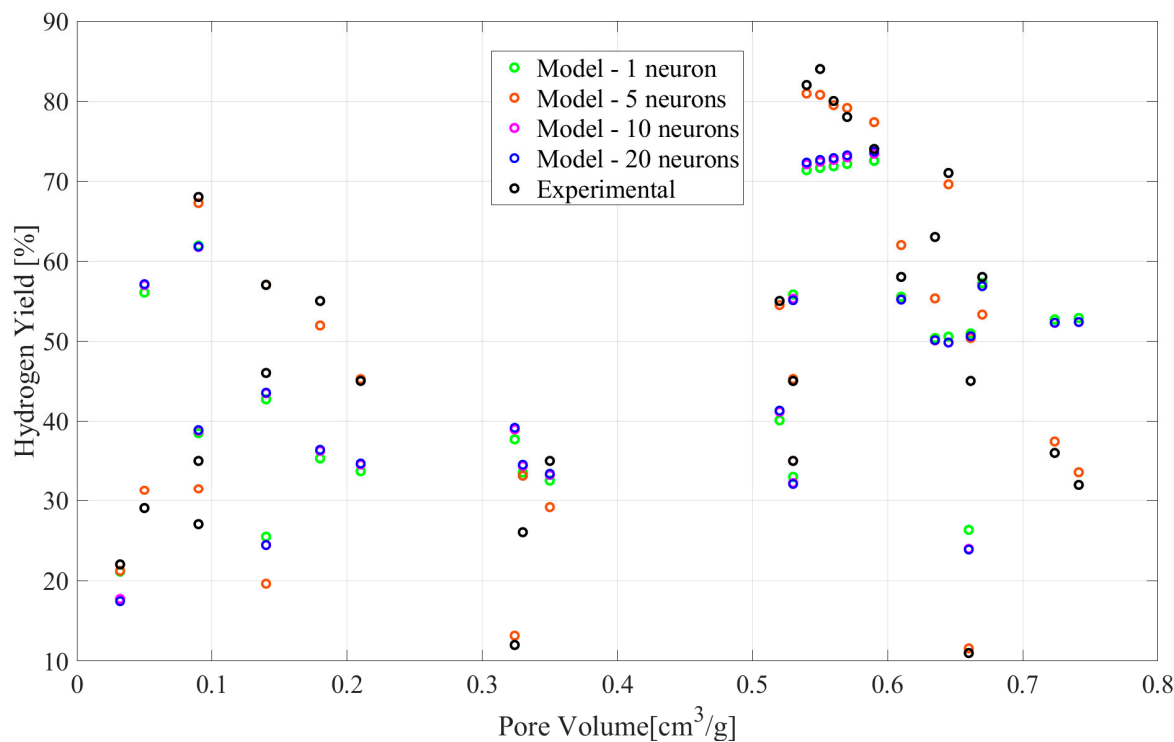


**Figure 8.** Experimental and ANN models using BR results of hydrogen yield as a function of pore volume.

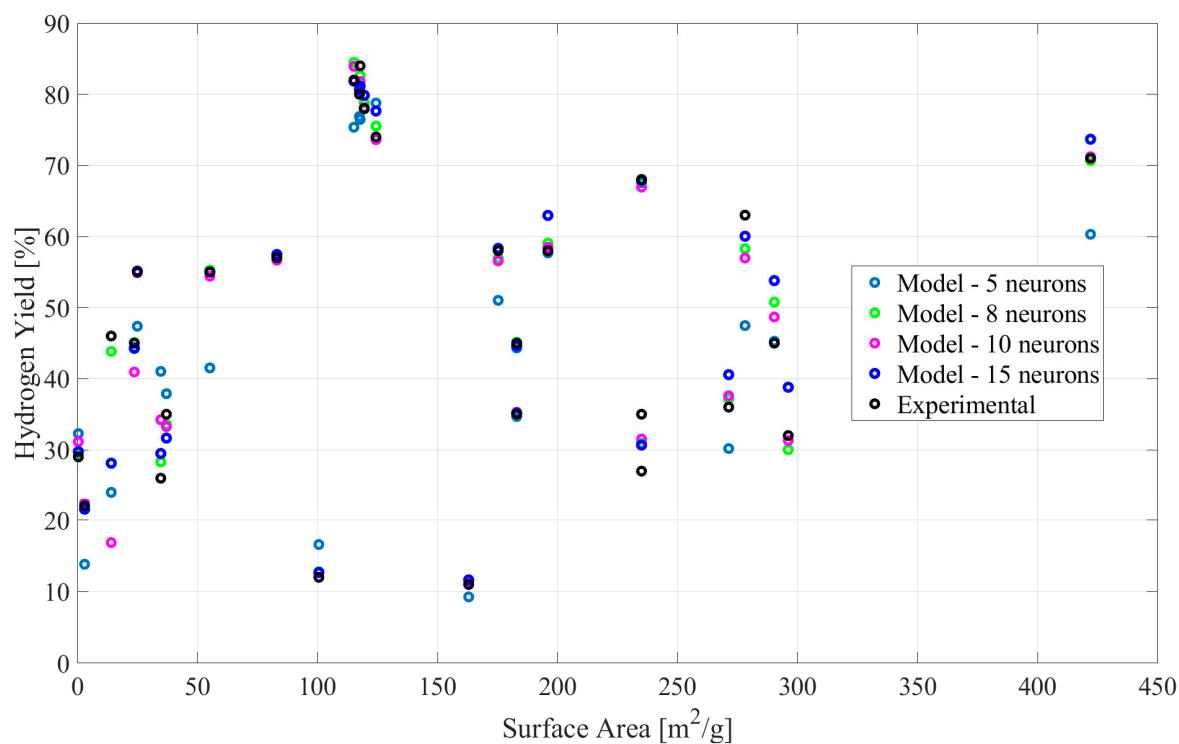


**Figure 9.** Experimental and ANN models using SCG results of hydrogen yield as a function of surface area.

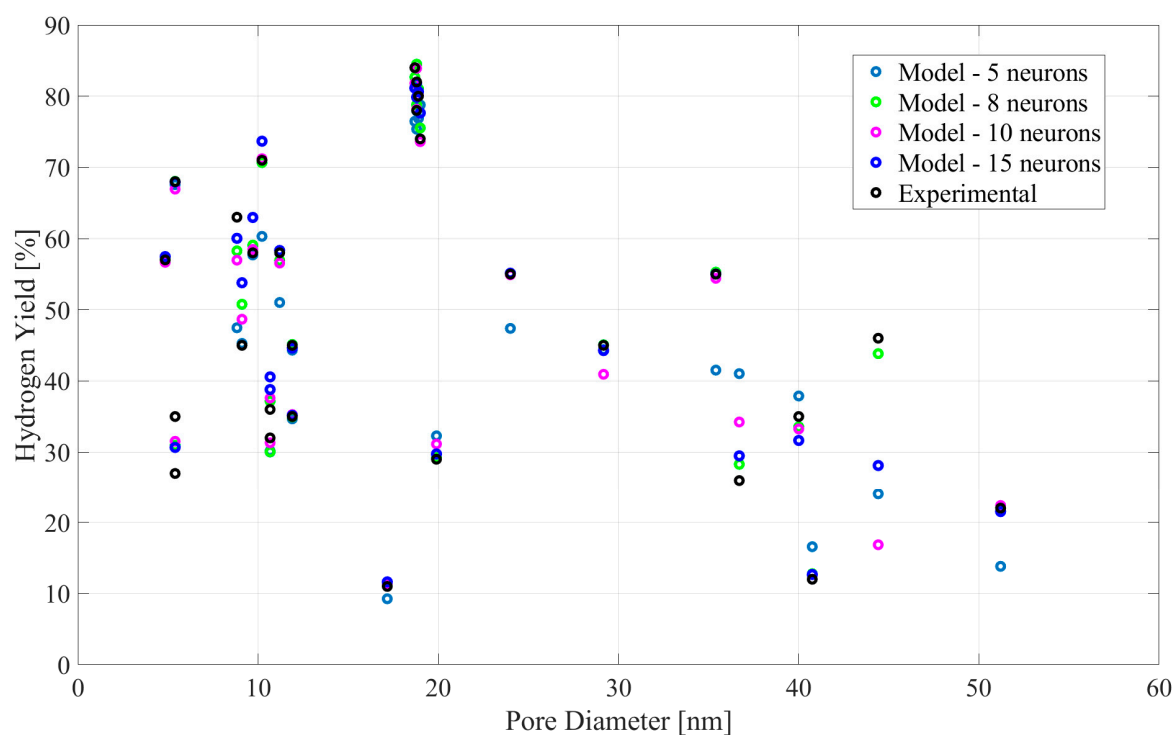


**Figure 10.** Experimental and ANN models using SCG results of hydrogen yield as a function of pore diameter.

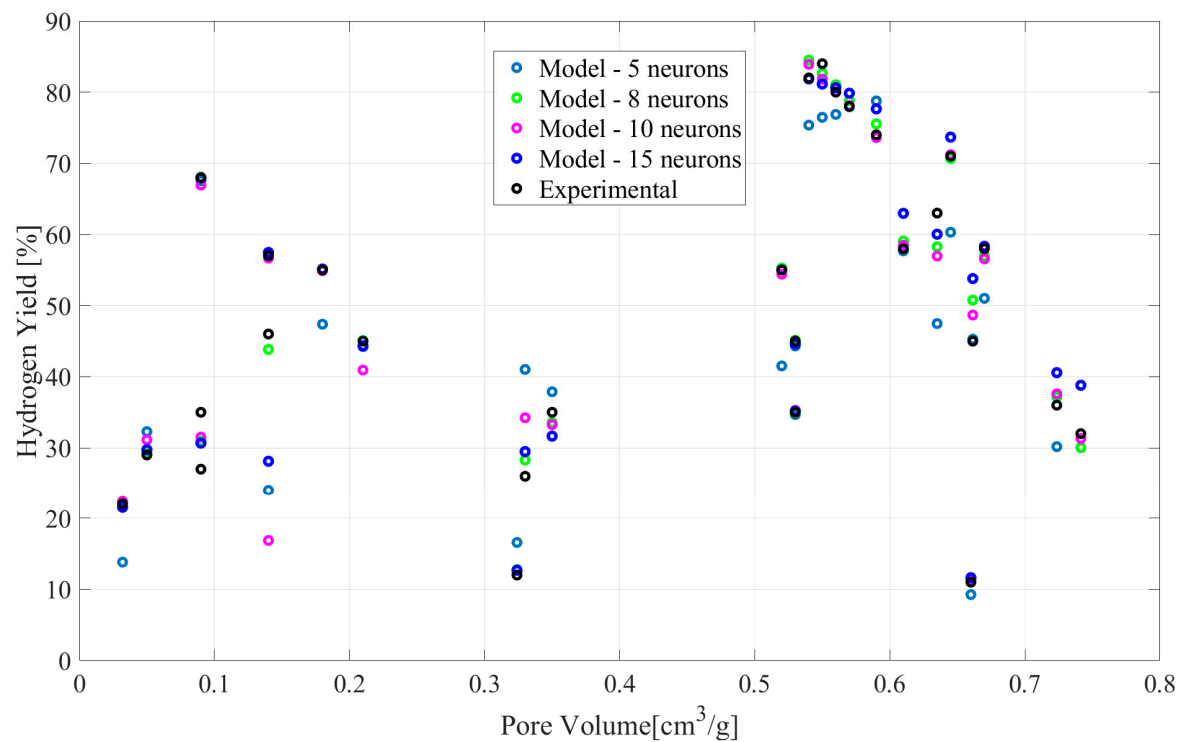


**Figure 11.** Experimental and ANN models using SCG results of hydrogen yield as a function of pore volume.

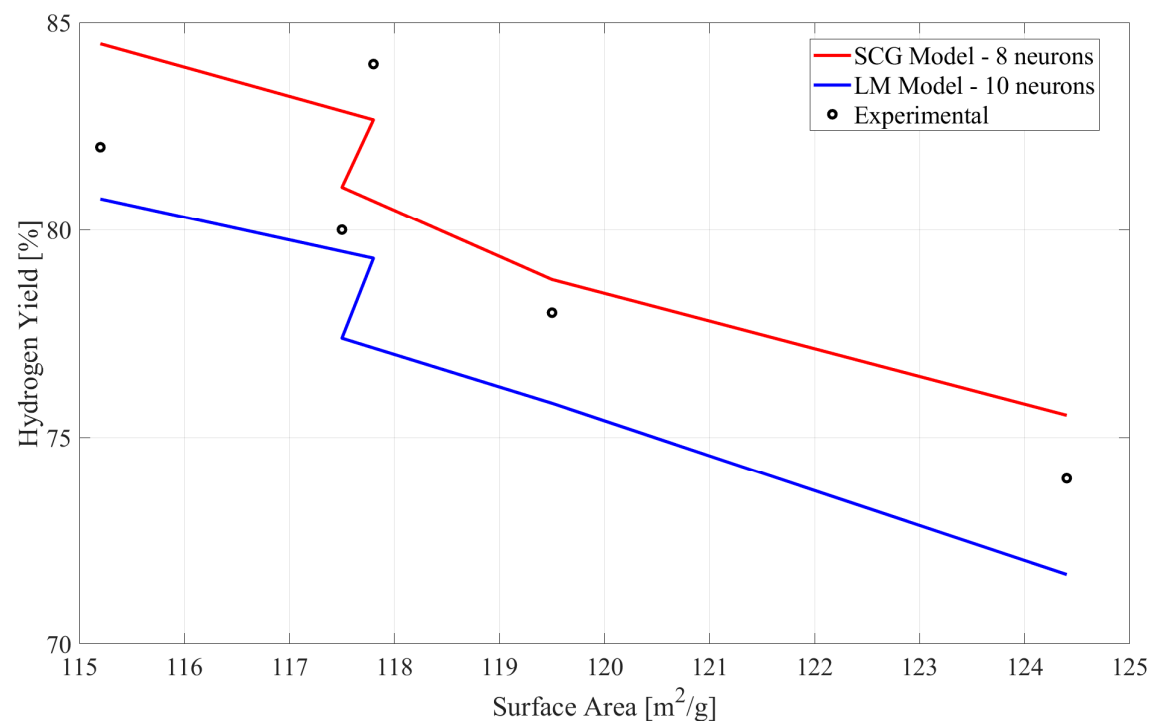


**Figure 12.** Experimental and optimal ANN models using SCG and LM as a function of surface at the given operating conditions.

Based on the model results, some of the developed models with different numbers of hidden neurons and learning algorithms can moderately estimate the experimental data. Models with a moderate number of hidden neurons (five to twenty) across all learning algorithms to achieve  $R^2$  values greater than 0.95 outperformed those with fewer or significantly more hidden neurons (less than five or more than twenty) with  $R^2$  values of 0.7 to 0.94, which are shown in the light orange highlighted rows in Table 2. A model with a smaller number of hidden neurons (such as one) is likely to have a poor fit compared to other models due to having fewer weights and biases. This is illustrated in Table 2, with the example of the ANN model with BR and one hidden neuron, which obtained a coefficient of determination of 0.7652, lower than 0.8, and an MSE of 180, which is remarkably high. An ANN model with an excessively high number of neurons (over 50) can experience overfitting, as evidenced by a relatively low coefficient of determination or a high MSE, as demonstrated by the ANN model with LM and 50 hidden neurons, which has an MSE value of 55.01. From Table 2, the best-fitting models are the ANN model using LM and ten hidden neurons, which had a coefficient of determination of 0.9931 and a mean squared error of 7.51, and the ANN model using SCG and eight hidden neurons, which had a coefficient of determination of 0.9951 and a mean squared error of 4.29. The optimal models are observed and compared with experimental data with varying surface areas at a constant temperature of 800 °C and GHSV of 42 L/h gcat, while the pore diameter is about 19 nm, and the pore volume is around 0.57 cm<sup>3</sup>/g, as shown in Figure 12. It can be observed that there is relatively close precision in terms of following the trend, and the accuracy is within 3% of the hydrogen yield, thus showing promise for the models to predict the hydrogen yield for DRM application.

The strong correlation between surface area and the hydrogen output of DRM can be observed in Figures 3, 6 and 9. The catalyst's surface area between 110 and 140 m<sup>2</sup>/g yields the maximum yield. These point clusters within this range also imply that it functions better for BR and LM when there are five neurons. All the model points for SCG, however, are nearer the experimental point. This also agrees with the literature that the increase in surface area, along with relatively higher operating temperature and GHSV, leads to higher catalytic activity and, thus, hydrogen production. The high surface area allows more active areas to be in close proximity to the reactants, therefore hastening the process. The more surface area catalysts provide for reactants to attach to them, the more opportunities for them to be more efficient. Greater surface area facilitates better distribution of the active ingredient, therefore preventing sticking together and maintaining a high activity level. A smaller surface area may result in fewer active sites, therefore reducing the catalyst's overall performance [3].

The effect of pore diameter is apparent in Figures 4, 7 and 10. All three types of models produced the highest yield when the pore diameter was around 18 nm, following the experimental value. This shows that the pore size, in this case diameter, plays an important role besides operating temperature and GHSV, where a relative decrease in diameter can lead to increased catalytic activity and DRM performance [3,20]. It could be that the decreased size in the diameter produced amorphous carbon species to result in the occurrence of the Boudouard reaction, resulting in higher hydrogen yield and lower carbon deposition. While smaller-width micropores can offer a lot of surface area, if they are too narrow, larger reactant molecules are not able to reach the active sites, limiting mass transfer. Mesopores or macropores facilitate products and reactants to pass through the material more easily, hence reducing diffusion resistance. This is particularly true for interactions involving larger molecules. For bigger compounds, this can strengthen the catalytic effect. The finest pore width depends on the size of the reactant molecules. While too small pores could make it difficult to reach or block, too large pores could shrink the surface area [3,23].

Figures 5, 8 and 11 show the effect of pore volume on hydrogen yield. These figures suggest that a high hydrogen yield can be obtained when the pore volume is between 0.52 and 0.60 cm<sup>3</sup>/g. The yield increases as pore capacity increases as a result of better

reactant diffusion. This value would decrease beyond an ideal pore volume. It is apparent in LM (Figure 5) that the yields are reduced when pore volume goes beyond 0.52 nm. LM rightly brings this trend. This shows again that the pore specific volume and size affect the catalytic activity and DRM performance, where the increase in pore volume results in higher DRM performance. Greater pore volume allows the catalyst to retain more reactants, therefore facilitating access to the active sites. It also makes it simple for goods to leave the pores, hence reducing the likelihood of pores becoming blocked. Nevertheless, if the pore volume is too large and the active surface area is insufficient, active sites could be lost [3,23].

It was observed from the literature that carbon deposition increases, hydrogen yield increases, and reactant conversion decreases are influenced by the pore volume, along with metal catalyst loading and support composition [23]. This trend is confirmed through this study. Although this study will benefit in predicting the DRM performance, it is mainly limited to similar types of DRM reactors due to the ANN modeling approach being an empirical model approach. More data on various reactors are needed to develop a more comprehensive model set.

A sensitivity analysis was conducted for the ANN and experimental models. This process helps understand how changes in input variables affect the output predictions. Using the dataset, the input perturbation method assessed the sensitivity of each input variable. This involves slightly varying each input by 1% deviation and observing the change in the output. Figure 13 shows that the temperature has the highest sensitivity, indicating that it is the most critical factor affecting the output. Moreover, pore diameter and surface area have moderate sensitivity to potentially play a significant role. Finally, pore volume and GHSV have lower sensitivity, indicating that they have less impact compared to other variables. Figure 14 visualizes the fitting of one of the ANN models using the LM algorithm, where the coefficient determination is illustrated on how the fit is compared and estimated.

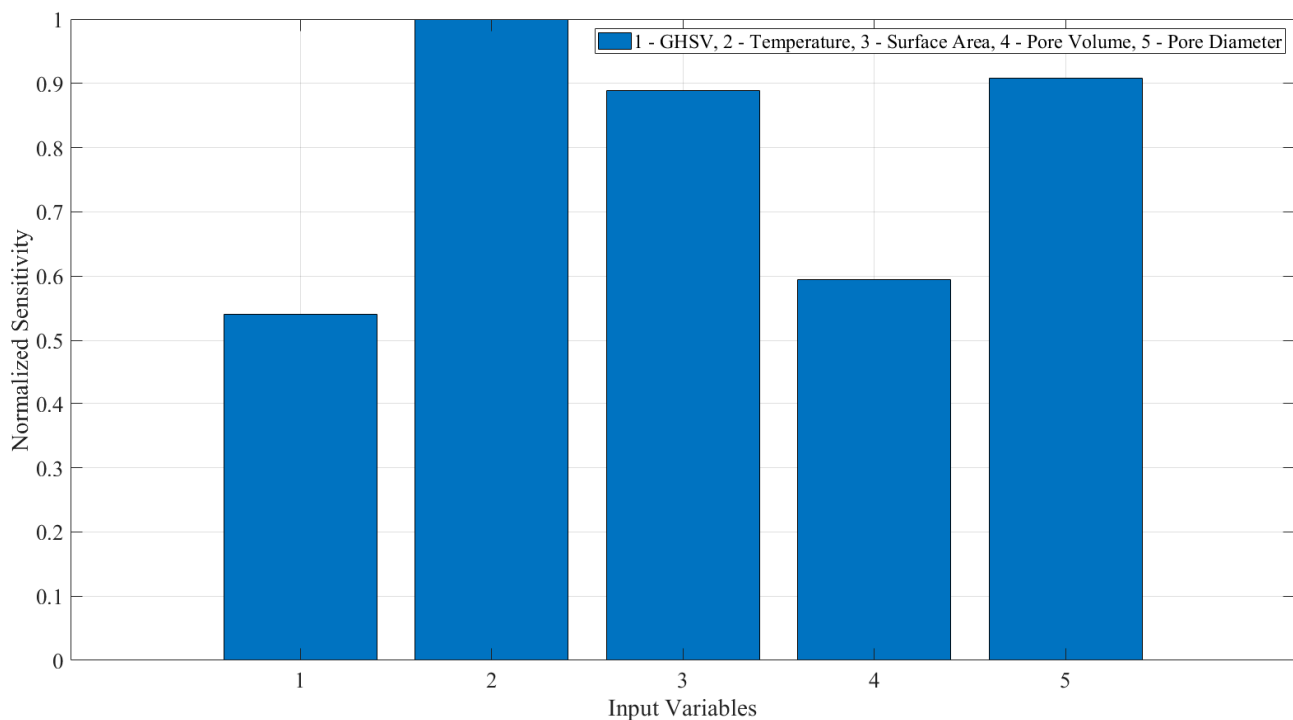


**Figure 13.** Sensitivity analysis of the ANN model and data for given input conditions.



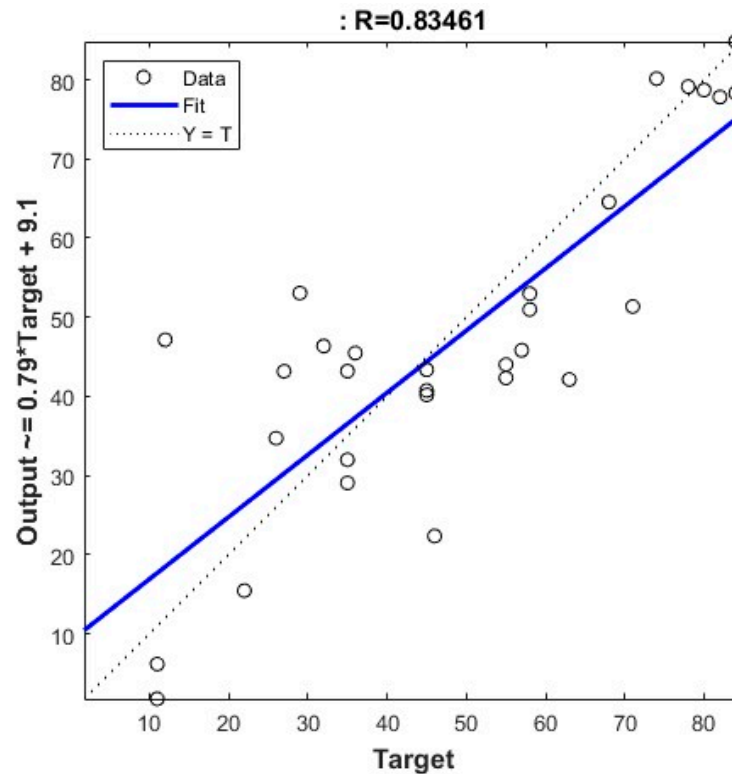


**Figure 14.** Fitting of the ANN model compared to target data for given input conditions using coefficient of determination.

#### 4. Conclusions

Given dry methane reforming is a feasible option to produce hydrogen effectively, this study uses experimental data to develop empirical models using ANN to predict hydrogen yield in the dry reforming of methane in the presence of nickel-based catalysts under different operating and physical conditions. Temperature, gas velocity, and three key geometric properties of the nickel-based catalysts were taken as input variables in the process of observing and predicting the hydrogen production yield from methane without the use of water. The ANN was trained using three different algorithms, Leven-Marquardt, Bayesian regularization, and scaled conjugate gradient, in order to forecast the hydrogen yield.

The ANN models that were best-fitting models involved ten hidden neurons and the LM algorithm, with an  $R^2$  of 0.9931 and an MSE of 7.51, and eight hidden neurons and the SCG algorithm, with an  $R^2$  of 0.9951 and an MSE of 4.29.

The hydrogen yield was relatively well-predicted when the ANN model was trained using the optimal number of hidden neurons and the learning algorithm. It is a sign that the measured measurements and the expected yield agree precisely. In order to examine the functional relationship between the hydrogen yield and variables in the hydrogen-generation process using a methane dry reforming reaction over a Ni-based catalyst, this work has shown how to employ ANN predictive modeling to be used to help design and optimize future DRM experiments based not only on thermal fluid properties but also geometric properties with relatively less time and resources utilized. This could lead to a more consistent and reliable performance of the DRM reactor that can be confidently monitored and assuredly controlled for high hydrogen yield to build up the amount of hydrogen to meet the clean energy market, including fuel cell electric vehicles and other applications. Further studies will be carried out by collecting and analyzing more relevant data for an optimized, comprehensive model.

Employing this developed model to describe the physical properties of catalysts could make it much easier to build and make new catalysts. This model could predict what

would happen and help with optimization by showing complex, non-linear connections between catalyst factors and their performance that would be hard to find with traditional testing methods. Experiments are used to teach this model how to predict what will happen when physical factors change in terms of catalyst activity. This ability to predict the future makes screening easier, improves performance, speeds up catalyst design, finds the best manufacturing parameters, cuts down on the time and cost of experiments, shows how complex interactions work, adapts to real-world conditions, and encourages catalyst design that is good for the environment.

This model will generate precise predictions regarding the performance of the catalyst as it is based on physical properties. The necessity for extensive experimentation will be diminished, and the cost will be reduced. It will tailor catalyst design efforts for specific industrial applications. Its application will accelerate the identification of high-performance catalysts, guaranteeing their optimization for both efficacy and longevity. This results in significant advancements in the industrial applications of dry methane reforming.

This study did not account for the catalytic support and the catalyst manufacturing process nor their implications on activity. Coke deposition was also not taken into account. A prospective modeling study may incorporate these characteristics based on available experimental results.

**Author Contributions:** Conceptualization, M.B. and M.H.R.; methodology, M.B. and M.H.R.; software, M.B.; validation, M.B. and M.H.R.; formal analysis, M.B. and M.H.R.; investigation, M.B. and M.H.R.; resources, M.B. and M.H.R.; data curation, M.H.R.; writing—original draft preparation, M.B. and M.H.R.; writing—review and editing, M.B. and M.H.R.; visualization, M.B. and M.H.R.; supervision, M.B. and M.H.R. All authors have read and agreed to the published version of the manuscript.

**Funding:** This project was funded by the National Plan for Science Technology and Innovation (MAARIFAH)—King Abdulaziz City for Science and Technology—the Kingdom of Saudi Arabia, Project number 11-ENV1786-08.

**Data Availability Statement:** The data presented in this study are openly available in article.

**Conflicts of Interest:** The authors declare no conflicts of interest.

## Nomenclature

Symbol/Acronym	Explanation
DRM	dry reformation of methane
ANN	artificial neural network
$\lambda_n$	scalar unit
GHSV	gas hourly space velocity
MSE	the mean squared error
$R^2$	coefficient of determination
$p$	data points occurring
$T$	prediction
$Z$	empirical data
$\bar{Z}$	the data averaged
SCG	scaled conjugate gradient
$\bar{w}$	vector in space
BR	Bayesian regularization
$g(w\alpha, M)$	the prior density
$g(Dw, \beta, M)$	the likelihood function

## References

1. Hosseini, S.E.; Wahid, M.A. Hydrogen Production from Renewable and Sustainable Energy Resources: Promising Green Energy Carrier for Clean Development. *Renew. Sustain. Energy Rev.* **2016**, *57*, 850–866. [[CrossRef](#)]
2. Chein, R.-Y.; Fung, W.-Y. Syngas Production via Dry Reforming of Methane over CeO<sub>2</sub> Modified Ni/Al<sub>2</sub>O<sub>3</sub> Catalysts. *Int. J. Hydrogen Energy* **2019**, *44*, 14303–14315. [[CrossRef](#)]

3. Usman, M.; Wan Daud, W.M.A.; Abbas, H.F. Dry Reforming of Methane: Influence of Process Parameters—A Review. *Renew. Sustain. Energy Rev.* **2015**, *45*, 710–744. [\[CrossRef\]](#)
4. Challiwal, M.S.; Ghouri, M.M.; Linke, P.; El-Halwagi, M.M.; Elbashir, N.O. A Combined Thermo-Kinetic Analysis of Various Methane Reforming Technologies: Comparison with Dry Reforming. *J. CO<sub>2</sub> Util.* **2017**, *17*, 99–111. [\[CrossRef\]](#)
5. Mourhly, A.; Khachani, M.; Kacimi, M.; Halim, M.; Arsalane, S. A New Low-Cost Mesoporous Silica as a Promising Support of Ni-Catalysts for High-Hydrogen Generation via Dry Reforming of Methane. In Proceedings of the 2017 International Renewable and Sustainable Energy Conference (IRSEC), Tangier, Morocco, 4–7 December 2017; IEEE: New York, NY, USA, 2017; pp. 1–7.
6. Zhang, G.; Liu, J.; Xu, Y.; Sun, Y. A Review of CH<sub>4</sub>/CO<sub>2</sub> Reforming to Synthesis Gas over Ni-Based Catalysts in Recent Years (2010–2017). *Int. J. Hydrogen Energy* **2018**, *43*, 15030–15054. [\[CrossRef\]](#)
7. Pan, C.; Guo, Z.; Dai, H.; Ren, R.; Chu, W. Anti-Sintering Mesoporous Ni–Pd Bimetallic Catalysts for Hydrogen Production via Dry Reforming of Methane. *Int. J. Hydrogen Energy* **2020**, *45*, 16133–16143. [\[CrossRef\]](#)
8. Kim, H.; Robertson, A.W.; Kwon, G.; O, J.W.; Warner, J.H.; Kim, J.M. Biomass-Derived Nickel Phosphide Nanoparticles as a Robust Catalyst for Hydrogen Production by Catalytic Decomposition of C<sub>2</sub>H<sub>2</sub> or Dry Reforming of CH<sub>4</sub>. *ACS Appl. Energy Mater.* **2019**, *2*, 8649–8658. [\[CrossRef\]](#)
9. Luyben, W.L. Design and Control of the Dry Methane Reforming Process. *Ind. Eng. Chem. Res.* **2014**, *53*, 14423–14439. [\[CrossRef\]](#)
10. Aouad, S.; Labaki, M.; Ojala, S.; Seelam, P.; Turpeinen, E.; Gennequin, C.; Estephane, J.; Aad, E.A. A Review on the Dry Reforming Processes for Hydrogen Production: Catalytic Materials and Technologies. In *Frontiers in Ceramic Science*; Cesario, M.R., Gennequin, C., Abi-Aad, E., De Macedo, D.A., Eds.; Bentham Science Publishers: Sharjah, United Arab Emirates, 2018; Volume 2, pp. 60–128, ISBN 978-1-68108-758-0.
11. Chaudhary, M.L.; Al-Fatesh, A.S.; Kumar, R.; Lanre, M.S.; Frusteri, F.; AlReshaidan, S.B.; Ibrahim, A.A.; Abasaeed, A.E.; Fakeeha, A.H. Promotional Effect of Addition of Ceria over Yttria-Zirconia Supported Ni Based Catalyst System for Hydrogen Production through Dry Reforming of Methane. *Int. J. Hydrogen Energy* **2022**, *47*, 20838–20850. [\[CrossRef\]](#)
12. Ahmed, H.; Alotibi, M.F.; Fakeeha, A.H.; Ibrahim, A.A.; Abasaeed, A.E.; Osman, A.I.; Al-Awadi, A.S.; Alarifi, N.; Al-Fatesh, A.S. Hydrogen Production via Methane Decomposition over Alumina Doped with Titanium Oxide-Supported Iron Catalyst for Various Calcination Temperatures. *ChemistryOpen* **2023**, *2023*, 00173. [\[CrossRef\]](#)
13. Alghamdi, A.M.; Ibrahim, A.A.; Ali, F.A.A.; Bamatraf, N.A.; Fakeeha, A.H.; Osman, A.I.; Alreshaidan, S.B.; Fadhillah, F.; Al-Zahrani, S.A.; Al-Fatesh, A.S. Tailored Ni-MgO Catalysts: Unveiling Temperature-Driven Synergy in CH<sub>4</sub>-CO<sub>2</sub> Reforming. *Catalysts* **2024**, *14*, 33. [\[CrossRef\]](#)
14. Abahussain, A.A.M.; Al-Fatesh, A.S.; Singh, S.K.; Almutairi, G.; Fakeeha, A.H.; Ibrahim, A.A.; Abasaeed, A.E.; Frusteri, L.; Labhasetwar, N.K. Cs Promoted Ni/ZrO<sub>2</sub>-Al<sub>2</sub>O<sub>3</sub> Catalysts for Dry Reforming of Methane: Promotional Effects of Cs for Enhanced Catalytic Activity and Stability. *Arab. J. Chem.* **2024**, *17*, 105564. [\[CrossRef\]](#)
15. Goula, M.A.; Charisiou, N.D.; Papageridis, K.N.; Delimitis, A.; Pachatouridou, E.; Iliopoulou, E.F. Nickel on Alumina Catalysts for the Production of Hydrogen Rich Mixtures via the Biogas Dry Reforming Reaction: Influence of the Synthesis Method. *Int. J. Hydrogen Energy* **2015**, *40*, 9183–9200. [\[CrossRef\]](#)
16. Sapi, A.; Rajkumar, T.; Abel, M.; Efremova, A.; Grossz, A.; Gyuris, A.; Abrahamne, K.B.; Szenti, I.; Kiss, J.; Varga, T.; et al. Noble-Metal-Free and Pt Nanoparticles-Loaded, Mesoporous Oxides as Efficient Catalysts for CO<sub>2</sub> Hydrogenation and Dry Reforming with Methane. *J. CO<sub>2</sub> Util.* **2019**, *32*, 106–118. [\[CrossRef\]](#)
17. Torrez-Herrera, J.J.; Korili, S.A.; Gil, A. Recent Progress in the Application of Ni-Based Catalysts for the Dry Reforming of Methane. *Catal. Rev.* **2023**, *65*, 1300–1357. [\[CrossRef\]](#)
18. Zhu, H.; Chen, H.; Zhang, M.; Liang, C.; Duan, L. Recent Advances in Promoting Dry Reforming of Methane Using Nickel-Based Catalysts. *Catal. Sci. Technol.* **2024**, *14*, 1712–1729. [\[CrossRef\]](#)
19. Kaneko, K. Determination of Pore Size and Pore Size Distribution: 1. Adsorbents and Catalysts. *J. Membr. Sci.* **1994**, *96*, 59–89. [\[CrossRef\]](#)
20. Leofanti, G.; Padovan, M.; Tozzola, G.; Venturelli, B. Surface Area and Pore Texture of Catalysts. *Catal. Today* **1998**, *41*, 207–219. [\[CrossRef\]](#)
21. Mashayekhi, F. The Effects of Molar Ratio and Calcination Temperature on NiO Nanoparticles’ Properties. *Int. Nano Lett.* **2022**, *12*, 273–279. [\[CrossRef\]](#)
22. Al-Fatesh, A.S.; Bamatraf, N.A.; Alreshaidan, S.B.; Abu-Dahrieh, J.K.; Patel, N.; Ibrahim, A.A.; Fakeeha, A.H.; bin Jumah, A.; Kumar, R. Cost-Effective Single-Step Synthesis of Metal Oxide-Supported Ni Catalyst for H<sub>2</sub>-Production Through Dry Reforming of Methane. *Arab. J. Sci. Eng.* **2024**, *49*, 8031–8047. [\[CrossRef\]](#)
23. Li, B.; Yuan, X.; Li, B.; Wang, X. Impact of Pore Structure on Hydroxyapatite Supported Nickel Catalysts (Ni/HAP) for Dry Reforming of Methane. *Fuel Process. Technol.* **2020**, *202*, 106359. [\[CrossRef\]](#)
24. Chen, W.; Nie, H.; Long, X.; Li, M.; Zhang, L.; Li, D. Role of Pore Structure on the Activity and Stability of Sulfide Catalyst. *Catal. Today* **2021**, *377*, 69–81. [\[CrossRef\]](#)
25. Yuan, P.; Liu, J.; Li, Y.; Fan, Y.; Shi, G.; Liu, H.; Bao, X. Effect of Pore Diameter and Structure of Mesoporous Sieve Supported Catalysts on Hydrodesulfurization Performance. *Chem. Eng. Sci.* **2014**, *111*, 381–389. [\[CrossRef\]](#)
26. Chen, L.; Qi, Z.; Zhang, S.; Su, J.; Somorjai, G.A. Catalytic Hydrogen Production from Methane: A Review on Recent Progress and Prospect. *Catalysts* **2020**, *10*, 858. [\[CrossRef\]](#)

27. Biswas, M.; Wilberforce, T.; Biswas, M.A. Prediction of Transient Hydrogen Flow of Proton Exchange Membrane Electrolyzer Using Artificial Neural Network. *Hydrogen* **2023**, *4*, 542–555. [CrossRef]
28. Alotaibi, F.N.; Berrouk, A.S.; Saeed, M. Optimization of Yield and Conversion Rates in Methane Dry Reforming Using Artificial Neural Networks and the Multiobjective Genetic Algorithm. *Ind. Eng. Chem. Res.* **2023**, *62*, 17084–17099. [CrossRef]
29. Griffin, W.O.; Darsey, J.A. Artificial Neural Network Prediction Indicators of Density Functional Theory Metal Hydride Models. *Int. J. Hydrogen Energy* **2013**, *38*, 11920–11929. [CrossRef]
30. Alsaffar, M.A.; Ghany, M.A.R.A.; Ali, J.M.; Ayodele, B.V.; Mustapa, S.I. Artificial Neural Network Modeling of Thermo-Catalytic Methane Decomposition for Hydrogen Production. *Top. Catal.* **2021**, *64*, 456–464. [CrossRef]
31. Hossain, M.A.; Ayodele, B.V.; Cheng, C.K.; Khan, M.R. Artificial Neural Network Modeling of Hydrogen-Rich Syngas Production from Methane Dry Reforming over Novel Ni/CaFe<sub>2</sub>O<sub>4</sub> Catalysts. *Int. J. Hydrogen Energy* **2016**, *41*, 11119–11130. [CrossRef]
32. Gendy, T.S.; El-Salamony, R.A.; Alrashed, M.M.; Bentalib, A.; Osman, A.I.; Kumar, R.; Fakeeha, A.H.; Al-Fatesh, A.S. Enhanced Predictive Optimization of Methane Dry Reforming via Response Surface Methodology and Artificial Neural Network Approaches: Insights Using a Novel Nickel-Strontium-Zirconium-Aluminum Catalyst. *Mol. Catal.* **2024**, *562*, 114216. [CrossRef]
33. Becker, S.; Karri, V. Predictive Models for PEM-Electrolyzer Performance Using Adaptive Neuro-Fuzzy Inference Systems. *Int. J. Hydrogen Energy* **2010**, *35*, 9963–9972. [CrossRef]
34. Biswas, M.A.R.; Robinson, M.D.; Fumo, N. Prediction of Residential Building Energy Consumption: A Neural Network Approach. *Energy* **2016**, *117*, 84–92. [CrossRef]
35. Wilberforce, T.; Biswas, M. A Study into Proton Exchange Membrane Fuel Cell Power and Voltage Prediction Using Artificial Neural Network. *Energy Rep.* **2022**, *8*, 12843–12852. [CrossRef]
36. Charisiou, N.D.; Siakavelas, G.; Tzounis, L.; Sebastian, V.; Monzon, A.; Baker, M.A.; Hinder, S.J.; Polychronopoulou, K.; Yentekakis, I.V.; Goula, M.A. An in Depth Investigation of Deactivation through Carbon Formation during the Biogas Dry Reforming Reaction for Ni Supported on Modified with CeO<sub>2</sub> and La<sub>2</sub>O<sub>3</sub> Zirconia Catalysts. *Int. J. Hydrogen Energy* **2018**, *43*, 18955–18976. [CrossRef]
37. Kurdi, A.N.; Ibrahim, A.A.; Al-Fatesh, A.S.; Alquraini, A.A.; Abasaeed, A.E.; Fakeeha, A.H. Hydrogen Production from CO<sub>2</sub> Reforming of Methane Using Zirconia Supported Nickel Catalyst. *RSC Adv.* **2022**, *12*, 10846–10854. [CrossRef]
38. Damyanova, S.; Shtereva, I.; Pawelec, B.; Mihaylov, L.; Fierro, J.L.G. Characterization of None and Yttrium-Modified Ni-Based Catalysts for Dry Reforming of Methane. *Appl. Catal. B Environ.* **2020**, *278*, 119335. [CrossRef]
39. Kumar, P.S.; Hogendoorn, J.A.; Feron, P.H.M.; Versteeg, G.F. New Absorption Liquids for the Removal of CO<sub>2</sub> from Dilute Gas Streams Using Membrane Contactors. *Chem Eng. Sci.* **2002**, *57*, 1639. [CrossRef]
40. Chaudhary, K.J.; Al-Fatesh, A.S.; Ibrahim, A.A.; Osman, A.I.; Fakeeha, A.H.; Alhoshan, M.; Alarifi, N.; Al-Muhtaseb, A.H.; Kumar, R. Enhanced Hydrogen Production through Methane Dry Reforming: Evaluating the Effects of Promoter-Induced Variations in Reducibility, Basicity, and Crystallinity on Ni/ZSM-5 Catalyst Performance. *Energy Convers. Manag. X* **2024**, *23*, 100631. [CrossRef]
41. Wille, J. On the Structure of the Hessian Matrix in Feedforward Networks and Second Derivative Methods. In Proceedings of the International Conference on Neural Networks (ICNN'97), Houston, TX, USA, 12 June 1997; Volume 3, pp. 1851–1855.
42. Lera, G.; Pinzolas, M. Neighborhood Based Levenberg-Marquardt Algorithm for Neural Network Training. *IEEE Trans. Neural Netw.* **2002**, *13*, 1200–1203. [CrossRef]
43. Møller, M.F. A Scaled Conjugate Gradient Algorithm for Fast Supervised Learning. *Neural Netw.* **1993**, *6*, 525–533. [CrossRef]
44. How Dynamic Neural Networks Work—MATLAB & Simulink. Available online: <https://www.mathworks.com/help/deeplearning/ug/how-dynamic-neural-networks-work.html> (accessed on 28 June 2024).

**Disclaimer/Publisher's Note:** The statements, opinions and data contained in all publications are solely those of the individual author(s) and contributor(s) and not of MDPI and/or the editor(s). MDPI and/or the editor(s) disclaim responsibility for any injury to people or property resulting from any ideas, methods, instructions or products referred to in the content.